Inorg. Chem. **2008**, *47*, 6427−6434

Role of Electronic Structure on DNA Light-Switch Behavior of Ru(II) Intercalators

Yujie Sun, Daniel A. Lutterman, and Claudia Turro*

Department of Chemistry, The Ohio State University, Columbus, Ohio 43210

Received March 28, 2008

A series of ruthenium(II) complexes possessing ligands with an extended π system were synthesized and characterized. The complexes are derived from $[Ru(bpy)_3]^{2+}$ (**1**, bpy = 2,2′-bipyridine) and include $[Ru(bpy)_2(tpphz)]^{2+}$ (**2**, tpphz = tetrapyrido[3,2-*a*:2′,3′-*c*:3″,2″-*h*:2‴,3‴-*j*]phenazine), $[Ru(bpy)_2(dppx)]^{2+}$ (**3**, dppx = 7,8-dimethyldipyrido[3,2-*a*:2′,3′-*c*]phenazine), $[Ru(bpy)_2(dppm2)]^{2+}$ (**4**, dppm2 = 6-methyldipyrido[3,2-*a*:2′,3′-*c*]phenazine), and $[Ru(bpy)_2(dppp2)]^{2+}$ (**5**, dppp2 = pyrido[2′,3′:5,6]pyrazino[2,3-*f*][1,10]phenanthroline). The excited-state properties of these complexes, including their DNA "light-switch" behavior, were compared to those of $[Ru(bpy)_2(dppz)]^{2+}$ (**6**, dppz = dipyrido[3,2-*a*:2′,3′-*c*]phenazine). Whereas **2**, **3**, and **4** can be classified as DNA light-switch complexes, **5** exhibits negligible luminescence enhancement in the presence of DNA. Because relative viscosity experiments show that **2**−**6** bind to DNA by intercalation, their electronic absorption and emission spectra, electrochemistry, and temperature dependence of the luminescence were used to explain the observed differences. The small energy gap between the lowest-lying dark excited state and the bright state in **2**−**4** and **6** is related to the ability of these complexes to exhibit DNA light-switch behavior, whereas the large energy gap in **5** precludes the emission enhancement in the presence of DNA. The effect of the energy gap among low-lying states on the photophysical properties of **1**−**6** is discussed. In addition, DFT and TD-DFT calculations support the conclusions from the experiments.

Introduction

Long-range charge transport in DNA has many potential applications,[1–5] including electrochemical sensors for specific DNA sequences,[6] hybridization,[7] and base pair mismatches,[8,9] among others.[10] The design of small molecules for sequence-specific DNA recognition has also been of interest owing to their potential role in sensitive diagnostics and chemotheraputics.[11–14] Ruthenium polypyridyl complexes are promising DNA probes due to their intense MLCT (metal-to-ligand charge transfer) luminescence and excited-state redox properties, together with their ability to bind to DNA.[15] Since the initial report that the nonemissive complex $[Ru(bpy)_2(dppz)]^{2+}$ (bpy = 2,2′-bipyridine, dppz = dipyrido[3,2-*a*:2′,3′-*c*]phenazine) emits brightly upon the addition of DNA, numerous related DNA "light-switch" complexes have been reported.[16–26] As discussed in more detail below, considerable attention has also been given to the investigation of the photophysical and electronic properties that give rise to the light-switch effect in this complex.[27–33]

* To whom correspondence should be addressed. E-mail: turro@chemistry.ohio-state.edu.

(1) Murphy, C. J.; Arkin, M. R.; Jenkins, Y.; Ghatlia, N. D.; Bossmann, S. H.; Turro, N. J.; Barton, J. K. *Science* **1993**, *262*, 1025.
(2) Kelley, S. O.; Barton, J. K. *Science* **1999**, *283*, 375.
(3) Delaney, S.; Yoo, J.; Stemp, E. D. A.; Barton, J. K. *Proc. Natl. Acad. Sci. U.S.A.* **2004**, *101*, 10511.
(4) O'Neill, M. A.; Barton, J. K. *Top. Curr. Chem.* **2004**, *236*, 67.
(5) Bjorklund, C. C.; Davis, W. B. *Nucleic Acids Res.* **2006**, *34*.
(6) Shao, F.; Augustyn, K.; Barton, J. K. *J. Am. Chem. Soc.* **2005**, *127*, 17445.
(7) Boon, E. M. *Nat. Biotechnol.* **2000**, *18*, 1096.
(8) Boon, E. M.; Barton, J. K. *Curr. Opin. Struct. Biol* **2002**, *12*, 320.
(9) Bichenkova, E. V.; Yu, X.; Bhadra, P.; Heissigerova, H.; Pope, S. J. A.; Coe, B. J.; Faulkner, S.; Douglas, K. T. *Inorg. Chem.* **2005**, *44*, 4112.
(10) Schuster, G. B. Long-Range Charge Transfer in DNA I & II. In *Top. Curr. Chem.*, Springer: 2004; Vol. 236−237.
(11) Odom, D. T.; Parker, C. S.; Barton, J. K. *Biochemistry* **1999**, *38*, 5155.
(12) Metcalfe, C.; Thomas, J. A. *Chem. Soc. Rev.* **2003**, *32*, 215.
(13) Boon, E. M.; Jackson, N. M.; Wightman, M. D.; Kelley, S. O.; Hill, M. G.; Barton, J. K. *J. Phys. Chem. B* **2003**, *107*, 11805.
(14) Rucker, V. C.; Dunn, A. R.; Sharma, S.; Dervan, P. B.; Gray, H. B. *J. Phys. Chem. B* **2004**, *108*, 7490.
(15) Kumar, C. V.; Barton, J. K.; Turro, N. J. *J. Am. Chem. Soc.* **1985**, *107*, 5518.
(16) (a) Moucheron, C.; Kirsch-De Mesmaeker, A.; Choua, S. *Inorg. Chem.* **1997**, *36*, 584. (b) Boisdenghien, A.; Moucheron, C.; Mesmaeker, K.-D. *Inorg. Chem.* **2005**, *44*, 7678.

10.1021/ic800560x CCC: $40.75
Published on Web 06/21/2008

$[Ru(bpy)_2(dppz)]^{2+}$ exhibits strong luminescence in a number of organic solvents, such as acetonitrile.[27,34–37] It was proposed that two or three Ru → dppz low-energy ^{3}MLCT excited states, the lowest of which is nonemissive, give rise to the DNA light-switch effect.[37–39] In water, the energy of the dark, nonemissive state is significantly lower than that of the bright, emissive state, such that the latter cannot be thermally accessed efficiently at room temperature.[37,38] In contrast, in organic solvents and when bound to DNA, the dark state lies just below the bright state in energy, resulting in thermal population of the latter at room temperature and strong luminescence.[37,38] It was proposed that the dark state stems from a transition from the Ru(II) center to the distal Ru (phz) portion of the dppz ligand, whereas the bright state arises from a transition from the metal to the proximal bpy part of the dppz ligand.[37,38] Consistent with observation, this model predicts a strong dependence of the emission intensity and lifetime of the complex on the environment and temperature.[37,38] It should be noted that previous reports placed the dark state above the bright state in aprotic solvents,[27] however, owing to the temperature dependence of the luminescence intensity and lifetime, it is now believed that the dark state is always lowest in energy.[37,38]

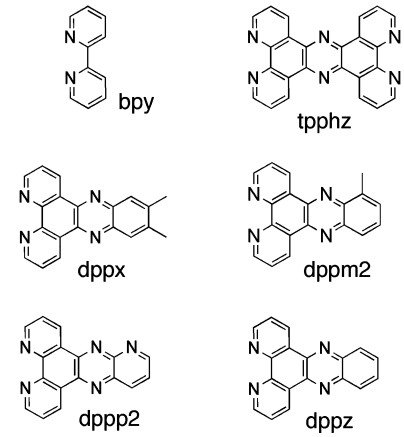

Figure 1. Molecular structures of L in the $[Ru(bpy)_2L]^{2+}$ complexes.

The synthesis and photophysical measurements of a series of ruthenium polypyridyl complexes $[Ru(bpy)_2L]^{2+}$ with L = dppx (7,8-dimethyldipyridophenazine), dppm2 (6-methyldipyridophenazine), dppa (dipyrido[3,2-*a*:2′,3′-*c*]phenazine-8-carboxylic acid), dppb (dipyrido[3,2-*a*:2′,3′-*c*]phenazine-8-benzaldehyde), dppp2 (pyrido[2′,3′:5,6]pyrazino[2,3-*f*][1,10]phenanthroline), dppp3 (pyrido[3′,4′:5,6]pyrazino[3,4-*f*][1,10]phenanthroline), and dppn (benzo[*i*]dipyrido[3,2-*a*:2′,3′-*c*]phenazine), were previously reported.[40] In addition to $[Ru(bpy)_2(dppz)]^{2+}$, $[Ru(bpy)_2L]^{2+}$ (L = dppx, dppm2, and dppa) exhibit luminescence enhancements by factors that range from 10 to 300 in the presence of DNA. In contrast, $[Ru(bpy)_2L]^{2+}$ (L = dppa, dppb, dppp2, dppp3, and dppn) display moderate enhancements (by factors that range from 1.3 to 2.0) upon binding to DNA.[40] Since all of the complexes are believed to bind to DNA via intercalation, it was proposed that the differences in photophysical properties in the presence of DNA are due to excited-state relaxation via an alternative nonemissive pathway in the latter, although experimental evidence for such mechanism was not provided.[40]

In the present work, $[Ru(bpy)_2L]^{2+}$ complexes with L = bpy (**1**), tpphz (**2**), dppx (**3**), dppm2 (**4**), and dppp2 (**5**) were synthesized and their photophysical properties were investigated (ligand structures shown in Figure 1). Electrochemistry, photophysical measurements, and theoretical calculations were performed to gain additional understanding of the differences in the excited-state manifolds of these complexes. For comparison, the light-switch prototype $[Ru(bpy)_2(dppz)]^{2+}$ (**6**) was also investigated (Figure 1). The results

(17) (a) Hartshorn, R. M.; Barton, J. K. *J. Am. Chem. Soc.* **1992**, *114*, 5919. (b) Holmlin, R. E.; Stemp, E. D. A.; Barton, J. K. *Inorg. Chem.* **1998**, *37*, 29. (c) Rueba, E.; Hart, J. R.; Barton, J. K. *Inorg. Chem.* **2004**, *43*, 4570.
(18) Arounaguiri, S.; Maiya, B. G. *Inorg. Chem.* **1999**, *38*, 842.
(19) (a) Zhang, Q. L.; Liu, J. H.; Ren, X. Z.; Xu, H.; Huang, Y.; Liu, J. Z.; Ji, L. N. *J. Inorg. Biochem.* **2003**, *95*, 194. (b) Tan, L. F.; Chao, H.; Li, H.; Liu, Y. J.; Sun, B.; Wei, W.; Ji, L. N. *J. Inorg. Biochem.* **2005**, *99*, 513.
(20) Sala, X.; Romero, I.; Rodriguez, M.; Llobet, A.; Gonzalez, G.; Martinez, M.; Benet-Buchholz, J. *Inorg. Chem.* **2004**, *43*, 5403.
(21) (a) O'Donoghue, K.; Penedo, J. C.; Kelly, J. M.; Kruger, P. E. *Dalton Trans.* **2005**, 1123. (b) O'Donoghue, K. A.; Kelly, J. M.; Kruger, P. E. *Dalton Trans.* **2004**, 13.
(22) Han, M. J.; Duan, Z. M.; Hao, Q.; Zheng, S. Z.; Wang, K. Z. *J. Phys. Chem. C* **2007**, *111*, 16577.
(23) Liu, Y.; Hammitt, R.; Lutterman, D. A.; Thummel, R. P.; Turro, C. *Inorg. Chem.* **2007**, *46*, 6011.
(24) Foxon, S. P.; Phillips, T.; Gill, M. R.; Towrie, M.; Parker, A. W.; Webb, M.; Thomas, J. A. *Angew. Chem., Int. Ed.* **2007**, *46*, 3686.
(25) Delgadillo, A.; Arias, M.; Leiva, A. M.; Loeb, B.; Meyer, G. J. *Inorg. Chem.* **2006**, *45*, 5721.
(26) Maheswari, P. U.; Rajendiran, V.; Stoeckli-Evans, H.; Palaniandavar, M. *Inorg. Chem.* **2006**, *45*, 37.
(27) Olson, E. J. C.; Hu, D.; Hormann, A.; Jonkman, A. M.; Arkin, M. R.; Stemp, E. D. A.; Barton, J. K.; Barbara, P. F. *J. Am. Chem. Soc.* **1997**, *119*, 11458.
(28) Lutterman, D. A.; Chouai, A.; Liu, Y.; Sun, Y.; Stewart, C. D.; Dunbar, K. R.; Turro, C. *J. Am. Chem. Soc.* **2008**, *130*, 1163.
(29) (a) Coates, C. G.; McGarvey, J. J.; Callaghan, P. L.; Coletti, M.; Hamilton, J. G. *J. Phys. Chem. B* **2001**, *105*, 730. (b) Coates, C. G.; Olofsson, J.; Coletti, M.; McGarvey, J. J.; Onfelt, B.; Lincoln, P.; Norden, B.; Tuite, E.; Matousek, P.; Parker, A. W. *J. Phys. Chem. B* **2001**, *105*, 12653. (c) Westerlund, F.; Pierard, F.; Eng, M. P.; Norden, B.; Lincoln, P. *J. Phys. Chem. B* **2005**, *109*, 17327. (d) Lundin, N. J.; Walsh, P. J.; Howell, S. L.; McGarvey, J. J.; Blackman, A. G.; Gordon, K. C. *Inorg. Chem.* **2005**, *44*, 3551.
(30) (a) Herman, L.; Elias, B.; Pierard, F.; Moucheron, C.; Kirsch-DeMesmaeker, A. *J. Phys. Chem. A* **2007**, *111*, 9756. (b) Pourtois, G.; Beljonne, D.; Moucheron, C.; Schumm, S.; Kirsch-De Mesmaeker, A.; Lazzaroni, R.; Bredas, J. L. *J. Am. Chem. Soc.* **2004**, *126*, 683.
(31) (a) Li, J.; Chen, J. C.; Xu, L. C.; Zheng, K. C.; Ji, L. N. *J. Organomet. Chem.* **2007**, *692*, 831. (b) Xu, L. C.; Li, J.; Shen, Y.; Zheng, K. C.; Ji, L. N. *J. Phys. Chem. A* **2007**, *111*, 273. (c) Li, J.; Xu, L. C.; Chen, J. C.; Zheng, K. C.; Ji, L. N. *J. Phys. Chem. A* **2006**, *110*, 8174.
(32) Wang, X.-y.; Del Guerzo, A.; Schmehl, R. H. *J. Photochem. Photobiol., C* **2004**, *5*, 55.
(33) Ghumaan, S.; Sarkar, B.; Patra, S.; vanSlageren, J.; Fiedler, J.; Kaim, W.; Lahiri, G. K. *Inorg. Chem.* **2005**, *44*, 3210.
(34) Nair, R. B.; Cullum, B. M.; Murphy, C. J. *Inorg. Chem.* **1997**, *36*, 962.
(35) Coates, C. G.; Callaghan, P. L.; McGarvey, J. J.; Kelly, J. M.; Kruger, P. E.; Higgins, M. E. *J. Raman Spectrosc.* **2000**, *31*, 283.
(36) Olofsson, J.; Wilhelmsson, L. M.; Lincoln, P. *J. Am. Chem. Soc.* **2004**, *126*, 15458.
(37) (a) Brennaman, M. K.; Meyer, T. J.; Papanikolas, J. M. *J. Phys. Chem. A* **2004**, *108*, 9938. (b) Brennaman, M. K.; Alstrum-Acevedo, J. H.; Fleming, C. N.; Jang, P.; Meyer, T. J.; Papanikolas, J. M. *J. Am. Chem. Soc.* **2002**, *124*, 15094.
(38) (a) Onfelt, B.; Lincoln, P.; Norden, B. *J. Am. Chem. Soc.* **2001**, *123*, 3630. (b) Olofsson, J.; Onfelt, B.; Lincoln, P. *J. Phys. Chem. A* **2004**, *108*, 4391.
(39) Batista, E. R.; Martin, R. L. *J. Phys. Chem. A* **2005**, *109*, 3128.
(40) Hartshorn, R. M.; Barton, J. K. *J. Am. Chem. Soc.* **1992**, *114*, 5919.

show a clear difference in the energies and the orbitals of contributions from the proximal and distal portions of the intercalating ligand to the low-lying MOs, resulting in different emissive character of the lowest-energy states among the complexes. These differences are more pronounced for **5**, which represents the only intercalator of the series that does not exhibit light-switch behavior.

Experimental Section

Materials. The ligands 2,2′-bipyridine (bpy), 1,10-phenanthroline, and precursors 1,2-diaminobenzene, 1,2-diamino-3-methylbenzene, 1,2-diamino-4,5-dimethylbenzene, and 2,3-diaminopyridine were purchased from Aldrich and used as received. Calf thymus DNA was purchased from Sigma and was dialyzed against 5 mM Tris buffer (50 mM NaCl, pH = 7.5) three times over a period of 48 h until $A_{260}/A_{280} > 1.8$, where A_{260} and A_{280} represent the absorbance at 260 and 280 nm, respectively.[41] $Ru(bpy)_2Cl_2$,[42] 1,10-phenanthroline- 5,6-dione (dione)[43,44] 5,6-diamino-1,10-phenanthroline,[43] $[Ru(bpy)_3](PF_6)_2$,[45] and $[Ru(bpy)_2(dione)](PF_6)_2$[46] were prepared according to literature methods. Complex **2** was prepared by the condensation of $[Ru(bpy)_2(dione)](PF_6)_2$ and 5,6-diamino-1,10-phenanthroline as previously reported,[47] and **3**−**6** were synthesized in a similar manner utilizing the corresponding *o*-diamines. The synthetic details and characterization are described in the Supporting Information, including ^{1}H NMR spectra (Figures S1−S6).

Instrumentation. ^{1}H NMR spectra were collected on a 400 MHz Bruker system, and MALDI-TOF mass spectrometry was performed on a Bruker Reflex III mass spectrometer with 2,5-dihyrdroxybenzoic acid as the matrix. Electronic absorption spectra were collected on a Hewlett-Packard diode array spectrometer (HP 8453) equipped with HP 8453 *WinSystem* software. Emission and excitation spectra were recorded on a SPEX Fluoromax-2 spectrometer with a 90° optical geometry equipped with a 150 W Xe arc lamp as the source. The temperature in the luminescence experiments was controlled by placing the sample in a quartz NMR tube within a quartz dewar, and a stream of cooled nitrogen gas was passed over the sample. The N_2 gas was allowed to flow through a 0.25 in. copper tube coil immersed in liquid nitrogen, and the temperature of the gas reaching the sample was tuned by varying its flow rate. The temperature was monitored by a thermocouple (OMEGA HH509) whose detector was submersed in the sample. Above 25 °C, the sample temperature was controlled by a NESLAB RTE-100 circulator connected to a jacketed cuvette holder using a mixture of ethylene glycol and water (v/v = 50:50) as the coolant. The temperature dependence of the emission is plotted as relative intensity versus *T*. The relative luminescence intensity is given by I_T/I_{max}, where I_T represents the integrated emission intensity at temperature *T* and I_{max} is the largest integrated intensity within the temperature change measured. Relative viscosity measurements were carried out on a Cannon-Manning Semi-Micro Viscometer immersed in a thermostatted water bath maintained at 24 ± 0.5 °C with a NESLAB RTE-100 circulator. Cyclic voltammograms were obtained on a Cypress Systems CS-1200 instrument.

Methods. Emission titrations were performed by maintaining the concentration of each Ru(II) complex constant at 10 μM and varying the concentration of calf-thymus DNA in 5 mM Tris buffer (pH 7.5, 50 mM NaCl). The DNA binding constants, K_b, were determined using the emission intensity of each complex bound to DNA (I_b), free in solution (I_f), and that which is apparent at each DNA concentration, I_a, by fitting plots of $(I_a - I_f)/(I_b - I_f)$ versus $[DNA]_t$, the total DNA concentration, to eq 1.[48,49]

$$\frac{I_a - I_f}{I_b - I_f} = \frac{b - (b^2 - 2K_b^2 C_t[DNA]_t/s)^{1/2}}{2K_b C_t} \quad (1)$$

In eq 1, $b = 1 + K_b C_t + K_b[DNA]_t/2s$, C_t represents the total complex concentration, and *s* is the base pair binding site size. The value of I_b was determined from the plateau of the titration, where additional DNA did not result in further changes to the emission intensity of each complex. For the relative viscosity measurements, the concentration of sonicated Herring sperm DNA was kept constant at 1 mM (5 mM Tris buffer, pH 7.5, and 50 mM NaCl) and the concentration of each metal complex was varied, such that *R* ([DNA]/[Ru]) = 0.05, 0.10, 0.15, 0.20, 0.25, 0.30. The change of the relative viscosity as a function of *R* was visualized by plotting $(\eta/\eta_o)^{1/3}$ versus *R*, where $\eta = t - t_o$ and $\eta_o = t_{DNA} - t_o$. In these relations, t_o, t_{DNA}, and *t* represent the flow times of the buffer alone, the DNA solution, and the DNA solution with the Ru(II) complex, respectively. The average of three measurements for each t_o, t_{DNA}, and *t* was used to calculate η and η_o.

Cyclic voltammograms were measured in a single-compartment three-electrode cell using distilled CH_3CN containing 0.1 M Bu_4NPF_6as the supporting electrolyte, a glassy carbon working electrode, a platinum wire auxiliary electrode, and a Ag/AgCl reference electrode. At the end of each experiment, a small amount of ferrocene (Fc) was added as an internal standard, and $E_{1/2}(Fc^{+/0}) = 0.66$ V versus NHE was used as reference for calculating the oxidation and reduction potentials of each complex.[47] Luminescence quantum yields were determined by integrating the corrected spectra over the frequency range of the emission of each complex using $[Ru(bpy)_3](PF_6)_2$ in CH_3CN as the standard ($\Phi_{em} = 0.062$).[50] Deoxygenation for the luminescence experiments was achieved by bubbling each solution with argon for ∼10 min and keeping it under positive argon pressure during the measurement.

The molecular and electronic structure calculations of **1**−**6** were performed with density functional theory (DFT) using the *Gaussian03* (*G03*) program package. The B3LYP functional[51] with the 6−31G* basis set was used for hydrogen, carbon, nitrogen, and oxygen[52] and the Stuttgart/Dresden (SDD) energy-consistent pseudopotentials for ruthenium.[53,54] All geometry optimizations were performed in either C_1 or C_2 symmetry with subsequent frequency analysis to show that the structures are at the local minima on the potential energy surface. Solvent effects were modeled by single-point calculations based on the gas phase optimized structures using

(41) Marmur, J. *J. Mol. Biol.* **1961**, *3*, 208.
(42) Sullivan, B. P.; Salmon, D. J.; Meyer, T. J. *Inorg. Chem.* **1978**, *17*, 3334.
(43) Bodige, S.; MacDonnell, F. M. *Tetrahedron Lett.* **1997**, *38*, 8159.
(44) Zhang, Z. B.; Yan, W. P.; Fan, M. G. *Chin. J. App. Chem.* **2005**, *22*, 103.
(45) Palmer, R. A.; Piper, T. S. *Inorg. Chem.* **1966**, *5*, 864.
(46) Goss, C. A.; Abruna, H. D. *Inorg. Chem.* **1985**, *24*, 4263.
(47) Bolger, J.; Gourdon, A.; Ishow, E.; Launay, J. P. *Inorg. Chem.* **1996**, *35*, 2937.
(48) Pyle, A. M.; Rehmann, J. P.; Meshoyrer, R.; Kumar, C. V.; Turro, N. J.; Barton, J. K. *J. Am. Chem. Soc.* **1989**, *111*, 3051.
(49) Nair, R. B.; Teng, E. S.; Kirkland, S. L.; Murphy, C. J. *Inorg. Chem.* **1998**, *37*, 139.
(50) Calvert, J. M.; Caspar, J. V.; Binstead, R. A.; Westmoreland, T. D.; Meyer, T. J. *J. Am. Chem. Soc.* **1982**, *104*, 6620.
(51) (a) Becke, A. D. *Phys. Rev. A: Gen. Phys.* **1988**, *38*, 3098. (b) Becke, A. D. *J. Chem. Phys.* **1993**, *98*, 5648.
(52) Hehre, W. J.; Radom, L.; Schleyer, P. v. R.; Pople, J. A. *Ab Initio Molecular Orbital Theory*; John Wiley & Sons: New York, 1986.
(53) Dolg, M.; Stoll, H.; Preuss, H. *Theor. Chim. Acta* **1993**, *85*, 441.
(54) Wedig, U.; Dolg, M.; Stoll, H. *Quantum Chemistry: The Challenge of Transition Metals and Coordination Chemistry*; Dordrecht: The Netherlands, 1986.

Table 1. Absorption Maxima, Molar Extinction Coefficients, Emission Maxima, Luminescence Quantum Yields, DNA Binding Constants, Halfwave Potentials (vs NHE), and HOMO-LUMO Energy Gaps from Calculation and Experiment of **2**−**6** Relative to **1**

complex	λ_{abs}/nm (ε/ × 10^{-4} $M^{-1}cm^{-1}$)[a]	λ_{em}/nm[b]	Φ_{em}[b]	K_b/M^{-1}[c]	$E_{1/2}$/V 3+/2+	2+/+	+/0	ΔE_{exptl}/V[d]	ΔE_{calcd}/eV[e]
1	243 (3.79), 286 (11.7), 452 (1.96)	619	0.062[f]	0.7×10^{3}[g]	1.54	−1.07	−1.26		
2	245 (5.63), 281 (10.7), 361 (1.94), 379 (2.60), 449 (1.72)	628	0.100	1.8×10^{6}	1.58	−0.74	−1.12	−0.29	−0.26
3	286 (13.9), 381 (2.83), 446 (2.27)	623	0.088	6.4×10^{6}	1.58	−0.77	−1.13	−0.26	−0.27
4	286 (14.5), 365 (2.39), 447 (2.28)	630	0.090	3.8×10^{7}	1.58	−0.74	−1.14	−0.29	−0.29
5	267 (11.2), 285 (12.7), 347 (3.65), 362 (4.73), 441 (2.88)	745	<0.005	[h]	1.60	−0.50	−1.16	−0.51	−0.52
6	284 (10.4), 320 (2.14), 359 (1.75), 370 (1.72), 445 (1.63)	631	0.083	$\geq 10^{6}$[i]	1.57[j]	−0.73[j]	−1.15[j]	−0.31	−0.33

[a] In water. [b] In CH_3CN. [c] From emission titration (Supporting Information). [d] $\Delta E_{exptl} = (E_{1/2}[Ru]^{3+/2+} - E_{1/2}[Ru]^{2+/+}) - (E_{1/2}[\mathbf{1}]^{3+/2+} - E_{1/2}[\mathbf{1}]^{2+/+})$, representing the difference of the experimental HOMO−LUMO gap compared to that of **1** (2.61 V). [e] Difference of calculated HOMO−LUMO gap compared to that of **1** (3.47 eV). [f] From ref 55. [g] From ref 47. [h] See text. [i] From ref 42. [j] From ref 58.

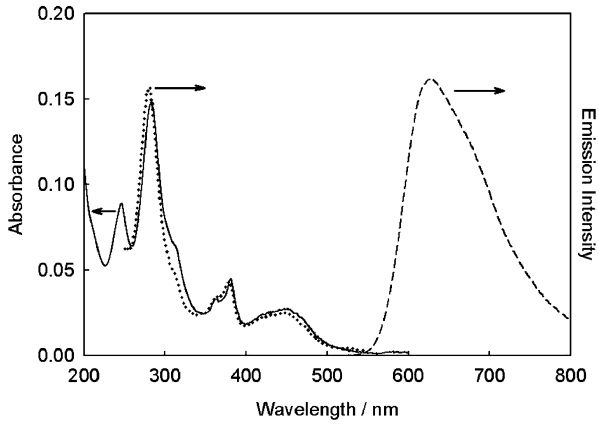

Figure 2. Electronic absorption (—), excitation (·····), and emission (− −) spectra of **2** (λ_{em} = 628 nm) at 298 K in CH_3CN.

the polarizable continuum model (PCM).[55] The orbital analysis was completed with *Molekel 4.3.win32*. The vertical singlet transition energies of the complexes were computed at the time-dependent density functional theory (TDDFT) level in water within *G03* using the ground-state optimized structure of each complex.

Results and Discussion

Electronic Absorption and Emission Spectra in Solution. In CH_3CN, $[Ru(bpy)_2(L)]^{2+}$ **2**−**6** exhibit the characteristic metal-to-ligand charge transfer (MLCT) absorption peaks arising from $Ru(t_{2g}) \rightarrow bpy(\pi^*)$ and $Ru(t_{2g}) \rightarrow L(\pi^*)$ transitions with maxima in the 430−450 nm range. As expected, the ligand-centered (LC) $\pi\pi^*$ transitions from the bpy ligands are observed between 281 and 286 nm in **1**−**6** (Table 1). In the 350−410 nm region, **2**−**6** exhibit $n\pi^*$ and $\pi\pi^*$ LC transitions localized on the ligand L that are not observed in **1** and whose energy and intensity depend on the identity of L.[40,47] As an example, the electronic absorption spectrum of **2** is shown in Figure 2.

The emission maxima (λ_{em}) of **1**−**6** in CH_3CN are also listed in Table 1, along with the corresponding luminescence quantum yields (Φ_{em}).[56] In a manner similar to **6**, complexes **2**, **3**, and **4** exhibit intense emission in CH_3CN at room temperature and weak luminescence in water. The emission quantum yields of **2**, **3**, and **4** were measured to be ∼0.1 in CH_3CN, consistent with previous reports.[40,57] In general, the emission maxima and intensities of light-switch complexes intercalated in DNA are very similar to those in CH_3CN.[17a,28] However, only weak emission was detected for **5** (Φ_{em} < 0.005) in the same solvent. The excitation spectra of **1**−**6** overlap well with the corresponding absorption spectra in CH_3CN, indicating that the luminescence of each complex arises from the lowest energy excited-state and that it does not originate from a highly emissive impurity. The absorption and excitation spectra of **2** are overlaid in Figure 2, and those collected for **1** and **3**−**6** are shown in the Supporting Information(Figures S7−S11).

Electrochemistry. The cyclic voltammograms of **1**−**6** in CH_3CN exhibit one reversible metal-based oxidation and several reversible ligand-centered reduction waves (Table 1). There is little variation in the oxidation potentials, $E_{1/2}([Ru]^{3+/2+})$, within the series, where [Ru] represents each complex. This result is expected for ruthenium(II) complexes with a metal-based HOMO possessing little contribution from the ligand L.[58,59] In contrast, the values of $E_{1/2}([Ru]^{2+/+})$ for **1**−**6** vary significantly with the identity of L. Complex **1** possesses the most negative $E_{1/2}([Ru]^{2+/+})$ value among the complexes, which is known to correspond to a bpy-localized reduction.[58,60] The $E_{1/2}([Ru]^{2+/+})$ values of **2**−**4** and **6** range from −0.73 to −0.77 V versus NHE, such that they are 0.30−0.34 V easier to be reduced than **1**. These values are consistent with the reduction being localized on the ligands with extended π structure, L, which are reduced more easily than bpy.[58] **5** is significantly easier to reduce than **2**−**4** and **6**, with $E_{1/2}([Ru]^{2+/+}) = -0.50$ V versus NHE. The dependence of $E_{1/2}([Ru]^{2+/+})$ on L and the first reduction being localized on the ligand that is easiest to reduce is typical of heteroleptic Ru(II) complexes of the type $[Ru(bpy)_2L]^{2+}$.[58]

In contrast, the second reduction potentials of **2**−**6**, $E_{1/2}([Ru]^{+/0})$ do not vary significantly among the complexes (Table 1). Similar results were previously reported for other heterolephic Ru(II) complexes,[57,58] including $[Ru(bpy)_2(taptp)]^{2+}$ (taptp = 4,5,9,18-tetraazaphenanthreno[9,10-*b*]triphenylene).[57] This invariance is not unexpected because the second reduction in these systems has been shown to place an electron on one of the ancillary bpy ligands.[47]

(55) (a) Fantacci, S.; De Angelis, F.; Selloni, A. *J. Am. Chem. Soc.* **2003**, *125*, 4381. (b) Fantacci, S.; De Angelis, F.; Sgamellotti, A.; Re, N. *Chem. Phys. Lett.* **2004**, *396*, 43.
(56) Caspar, J. V.; Meyer, T. J. *J. Am. Chem. Soc.* **1983**, *105*, 5583.
(57) Liu, Y.; Chouai, A.; Degtyareva, N. N.; Lutterman, D. A.; Dunbar, K. R.; Turro, C. *J. Am. Chem. Soc.* **2005**, *127*, 10796.
(58) Juris, A.; Balzani, V.; Barigelletti, F.; Campagna, S.; Belser, P.; Von Zelewsky, A. *Coord. Chem. Rev.* **1988**, *84*, 85.
(59) Fees, J.; Kaim, W.; Moscherosch, M.; Matheis, W.; Klima, J.; Krejcik, M.; Zalis, S. *Inorg. Chem.* **1993**, *32*, 166.
(60) Elliott, C. M.; Hershenhart, E. J. *J. Am. Chem. Soc.* **1982**, *104*, 7519.

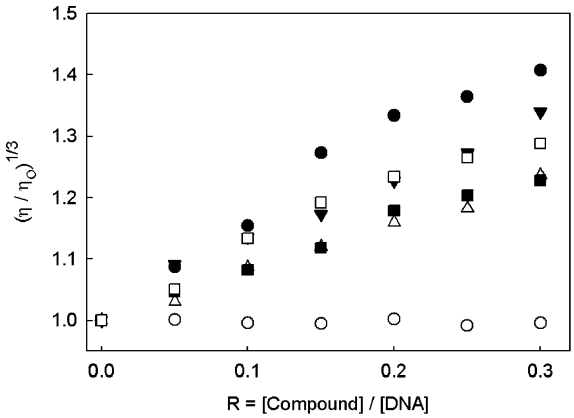

Figure 3. Relative viscosity plot of $(\eta/\eta_o)^{1/3}$ vs R (R = [compound]/[DNA]) for ethidium bromide (●), **1** (○), **2** (▼), **3** (△), **4** (■), and **5** (□) at 24 ± 1 °C in 5 mM Tris (50 mM NaCl, pH 7.5).

DNA Binding and DNA Light-Switch Behavior. It is generally believed that intercalation is important for DNA light-switch behavior. Therefore, it is necessary to investigate whether the differences in photophysical properties of the complexes are a result of variations in the DNA binding mode. The DNA binding constants, K_b, of **1**−**6**, were determined from fits of the changes in the emission intensity of each complex as a function of increasing DNA concentration to eq 1, which resulted in the values listed in Table 1. The emission titration plots for **2**−**4** are shown in Figure S12 (Supporting Information). These DNA binding constants are of similar magnitude to that of **6**, which are 3−4 orders of magnitude greater than that of **1**.[48,61] Because there is only weak luminescence enhancement observed for **5** in the presence of DNA, it was not possible to obtain a DNA binding constant using this method. Attempts to measure the value of K_b for **5** from absorption titrations were also unsuccessful. It should be noted that the emission of **5** is not quenched in the presence of DNA, as is the case for complexes with excited states that are able to oxidize guanine. A 9-fold emission intensity increase was observed for **5** in the presence of excess calf-thymus DNA, whereas only a 2-fold increase was observed for the complex in the presence of duplex poly(dA:dT), showing that guanine does not quench the emission of **5**. However, the magnitude of the luminescence enhancement of **5** is modest compared to **2**−**4**, which exhibit increases in the emission intensity by factors that range from 110-fold to 340-fold in the presence of DNA.

The values of K_b obtained using eq 1 do not provide conclusive evidence of the binding mode of the complexes, since intercalation, groove binding, and hydrophobic interactions may also result in an increase in the emission intensity.[40] Relative viscosity measurements are known to be a reliable technique to establish DNA intercalation.[62] The relative viscosity changes of DNA solutions upon addition of **2**−**5** demonstrate that these complexes are intercalators (Figure 3), similar to previous reports for **6**.[43] As expected for a non-intercalator, the relative viscosity of the DNA solution is independent of the concentration of **1**. However, it does increase as a function of ethidium bromide, a well-known intercalator (Figure 3). The relative viscosity at each complex concentration is greater for **2** and **5** than for **3** and **4**, indicating better intercalation in the former than in the latter. This difference may be due to the steric hindrance provided by the methyl substituents in **3** and **4**.

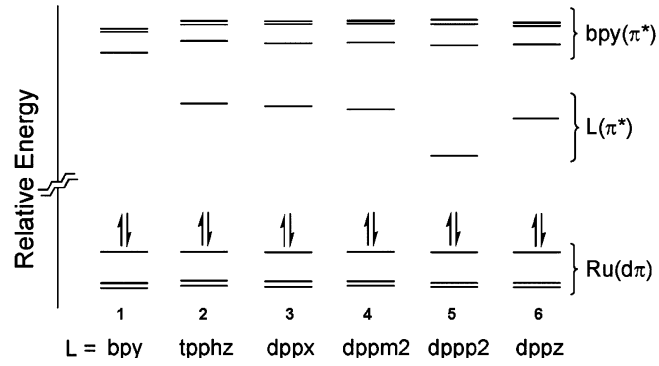

Figure 4. Molecular orbital diagrams comparing the relative energies of the frontier orbitals in **1**−**6**, showing MOs centered on the metal, Ru(dπ), those with contributions on the distal portion of L, L(π*), and those localized on the bpy portion of L or the two ancillary bpy ligands, bpy(π*).

The relative viscosity measurements clearly show that differences in the DNA binding mode can be ruled out as the source of the different photophysical properties of these complexes in the presence of DNA, since **2**−**6** are all DNA intercalators. Therefore, it may be concluded that the lack of light-switch behavior reported for **5** is not related to the DNA binding mode of the complex.

Electronic Structure Calculations. DFT calculations were performed to aid in the interpretation of the differences in the excited-state behavior of **1**−**6**. A set of three occupied metal-centered MOs is comprised of the highest occupied molecular orbital (HOMO), as well as the HOMO−1 and HOMO−2 of **1** (Figure 4); these occupied orbitals will be referred to as the Ru(dπ) set. Because the same set of three Ru(dπ) orbitals were also calculated for **2**−**6**, the energies of the HOMOs for **1**−**6** were set equal to 0 eV (Figure 4). Setting the HOMOs in all the complexes to the same energy is supported experimentally by the invariance in the oxidation potentials of **1**−**6** (Table 1).

The lowest unoccupied molecular orbital (LUMO) for **1** was calculated to possess bpy(π*) character (Figure 4), consistent with previous reports.[63,64] The LUMOs of **2**−**6** were found to be L(π*) in character (Figure 4), with the orbital contributions centered on the distal portion of each ligand L. The MOs that comprise the LUMO, LUMO+1, and LUMO+2 of **1**−**6** are shown in the Supporting Information (Table S1). The calculated LUMOs of **2**−**4** lie 3.18 to 3.21 eV above the Ru(dπ) HOMO, which are similar to the 3.14 eV HOMO−LUMO gap calculated for **6**. The LUMOs of **2**−**4** and **6** were calculated to be ~0.3 eV lower in energy than the LUMO of **1** (Figure 4). The energy differences between the HOMO−LUMO gaps of **2**−**6** and that of **1** are listed as ΔE_{calcd} in Table 1. These values are

(61) Jenkins, Y.; Friedman, A. E.; Turro, N. J.; Barton, J. K. *Biochemistry* **1992**, *31*, 10809.
(62) Lerman, L. S. *J. Mol. Biol.* **1961**, *3*, 18.
(63) Charlot, M. F.; Pellegrin, Y.; Quaranta, A.; Leibl, W.; Aukauloo, A. *Chem.—Eur. J.* **2006**, *12*, 796.
(64) Nozaki, K.; Takamori, K.; Nakatsugawa, Y.; Ohno, T. *Inorg. Chem.* **2006**, *45*, 6161.

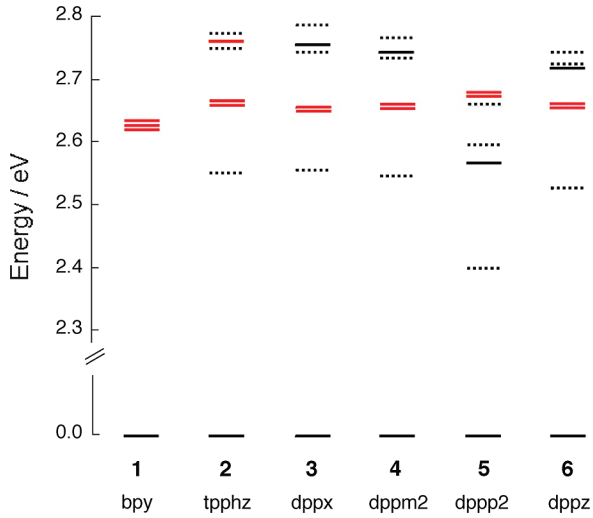

Figure 5. Energies of the singlet excited states calculated for **1**−**6** (red = emissive, black = nonemissive, dashed = both emissive and nonemissive contributions).

in agreement with that of the measured differences between $E_{1/2}([Ru]^{2+/1+})$ and $E_{1/2}([Ru]^{3+/2+})$ values of **2**−**4** and **6**, which correspond to the experimentally measured HOMO−LUMO gap, relative to the same difference for **1**, listed as ΔE_{exptl} in Table 1. It should be noted that the HOMO−LUMO gap of **5** was calculated to be 0.52 eV smaller than that of **1** (Figure 4), a finding that also agrees with the electrochemical data, for which $\Delta E_{exptl} = 0.51$ V (Table 1). This agreement between the calculated and experimental results shows that the theoretical calculations provide reliable information on the electronic structures of these complexes.

Time-dependent DFT (TD-DFT) calculations result in the vertical singlet excited states for **1**−**6** shown in Figure 5. The energies, transition contributions, and weighting factors of calculated singlet excited states for **1**−**6** are listed in Tables S2−S7 (Supporting Information). The lowest-energy ^{1}MLCT state of **1** was calculated at 2.62 eV ($f = 0.0017$, 473 nm) and the corresponding ^{3}MLCT state is expected to lie ∼0.62 eV (∼5,000 cm^{-1}) below the ^{1}MLCT at 2.00 eV (620 nm).[74] Four ^{1}MLCT states of **1** with significant oscillator strength were calculated between 419−437 nm ($0.0136 < f < 0.1243$), consistent with the broad MLCT absorption of the complex with maximum at 452 nm (Table S2, Supporting Information). The relative energies of the three lowest-lying singlet excited states of **1** are shown in Figure 5, together with those of **2**−**6**. The calculations show that for **1**−**6**, all low-lying singlet excited states are MLCT in character. Similarly, **2**−**4** and **6** exhibit the lowest ^{1}MLCT state at 485−491 nm with $f < 0.0001$ (Tables S3−S5 and S7, Supporting Information). In these complexes, the ^{1}MLCT with $f \sim 0.1$ is calculated at 449−456 nm, consistent with the corresponding experimental MLCT absorption maxima (Tables S3−S5 and S7, Supporting Information). It is apparent from Table S6 that the lowest energy ^{1}MLCT excited state for **5** is calculated at 517 nm ($f = 0.0005$), and excited states with significant oscillator strength are found at 483 nm ($f = 0.0497$), 416 nm ($f = 0.1282$), and 414 nm ($f = 0.1352$). The discussion below focuses on the emission of the complexes from the ^{3}MLCT state(s). Assuming that the energy gap between the lowest ^{1}MLCT and ^{3}MLCT of **2**−**6** is similar as that of **1**, we approximate here that each ^{3}MLCT state lies 5000 cm^{-1} below its corresponding ^{1}MLCT state for **2**−**6** (energies listed as λ_{trip} in Tables S2−S7, Supporting Information), such that the relative order of the MLCT states does not vary from the singlet to the triplet manifolds.[58]

It has been proposed that the luminescence observed from **6** arises from the thermal population of the ^{3}MLCT emissive excited state that lies above the lowest energy nonemissive ^{3}MLCT state and that the energy difference between these states is dependent on the surrounding medium and results in the variation of the luminescence intensity.[37] In addition, it was proposed that the lowest energy nonemissive state in **6** arises from a ^{3}MLCT transition from the Ru(II) to the phenazine (phz) part of the dppz ligand, whereas the emissive state is a result of charge transfer from the metal center to the bpy portion of the same ligand or the ancillary bpy ligands. Similarly, those states with transitions from the metal center to the distal portion of the extended π system of the ligand L in **2**−**5** are expected to be nonemissive, whereas those states with transitions to the two ancillary bpy ligands or the bpy portion of L are expected to be emissive. These criteria were used to determine whether states are emissive (bright, BS), nonemissive (dark, DS), or to possess mixed-emissive character (mixed, MS) in Figure 5. It should be noted that dark states possessed >75% of transitions expected to be nonemissive (determined from the weighing factors), and bright states contained 100% emissive transitions. States that did not fit these criteria were labed mixed.

For **2**−**6**, the electron density of each LUMO is localized on the distal portion of the ligand L (Table S1, Supporting Information). In contrast, the electron density of the LUMO+1, LUMO+2, and LUMO+3 in **2**−**6** are localized on the portion of L proximal to the metal or on the ancillary bpy ligands. Therefore, it is expected that transitions from the ruthenium center to the LUMOs of **2**−**6** will result in nonemissive or weakly emissive MLCT excited states, whereas MLCT excited states involving the LUMO+1, LUMO+2, and LUMO+3 should be emissive. All of the MLCT excited states of **1** are assigned as emissive and are shown as red lines in Figure 5. However, as shown in Table S7 (Supporting Information), the lowest singlet excited state (^{1}ES$_1$) of **6** possesses contributions of transitions from the HOMO to the LUMO, LUMO+1, and LUMO+2, giving this excited state mixed emissive and nonemissive character. States such as the ^{1}ES$_1$ of **6** with mixed character are shown as dashed lines in Figure 5 to indicate that it has both emissive and nonemissive contributions. At energies greater than that of ^{1}ES$_1$, both the ^{1}ES$_2$ (2.65 eV) and ^{1}ES$_3$ (2.66 eV) of **6** are expected to be emissive. Assuming a similar singlet−triplet gap as in **1** (∼5000 cm^{-1}), the corresponding emissive ^{3}MLCT of **6** is expected to be at ∼2.04 eV (608 nm), which agrees well with the emission maximum of **6** at 628 nm (Table 1). The lowest-energy excited states of **2**−**4** also possess both emissive and nonemissive contributions (Figure 5), with two emissive states at energies greater than that of ^{1}ES$_1$ (Tables S3−S5, Supporting Information). The

expected energy of the emissive ^{3}MLCT state for each complex matches well with their corresponding experimental maxima (Table 1). Although the lowest energy excited-state in **2**−**4** and **6** is expected to have mixed-emissive character, it is likely that emission from this state is not observed because of its very low quantum yield compared to the bright state of each complex.

Similar to **2**−**4** and **6**, the lowest-energy excited state of **5**, $^1ES_1$, is predicted to have contributions from both emissive and nonemissive transitions (Tables S3−S7, Supporting Information). A nonemissive state, $^1ES_2$, and two mixed-character states, $^1ES_3$ and $^1ES_4$, are calculated to lie 0.17 eV, 0.19 eV, and 0.26 eV, respectively, above the $^1ES_1$ state in **5**. In contrast, in **2**−**4** and **6** only emissive states are present 0.11 to 0.14 eV above each corresponding $^1ES_1$ excited state (Figure 5). The calculations reveal that the weak emission of **5** with maximum at 745 nm in CH_3CN may be attributed to the lowest energy excited state in **5** ($^3ES_1$ at 697 nm), which is observable in the absence of nearby highly emissive state(s). It should also be noted that there are two emissive excited states, $^1ES_5$ and $^1ES_6$, predicted to lie 0.27 eV above $^1ES_1$ in **5**, at approximately the same energy as the emissive states of **1**−**4** and **6** (Figure 5). The results from the calculations show clear differences in the excited-state manifolds of the DNA light-switch complexes (**2**−**4** and **6**) and that of **5**, the only complex in the series that is not a light-switch.

Temperature Dependence of the Emission. In addition to solvent, temperature has also been shown to affect the emission intensity of **6** by varying the relative populations of the emissive and weakly or nonemissive excited states according to the Boltzmann distribution.[37,39,65] Therefore, the temperature dependence of the emission intensity of **2**−**6** can provide information regarding the energy difference between emissive and nonemissive excited states in these complexes.

The changes in the luminescence intensity of each complex as a function of temperature in ethanol are shown in Figure 6. The luminescence intensity of **1** increases with decreasing temperature from 325 to 265 K, and remains relatively constant from 265 to 195 K, consistent previously reports.[50] However, the luminescence of **6** increases with temperature from 190 to 305 K, followed by a decrease in luminescence from 305 to 332 K. Therefore, the maximum intensity is observed at 305 K for **6**, making it the roll-over temperature of the complex, in agreement with literature data.[37] Complexes **2**−**4** exhibit similar behavior (Figure 6), with roll-over temperatures of 273 K for **2** and 285 K for **3** and **4**, such that the roll-over temperatures of **2**−**4** are ∼30 K below that of **6**. The similarity in the roll-over temperatures of **3** and **4** indicates that the position of the methyl substituents on the dppz ligand does not significantly affect the electronic structure of the complexes.

The temperature dependence of the luminescence is consistent with the presence of two (or more) ^{3}MLCT excited states in **2**−**4** and **6**, where one or more of these states are nonemissive or very weakly emissive (mixed-state) and the other(s) are bright (emissive), with the mixed state(s) lower in energy than the bright state(s). Because the nonemissive ^{3}dd state(s) are located above the bright ^{3}MLCT state(s), it is expected that there may be two equilibria, one between the nonemissive ^{3}dd (Ru) state(s) and the bright ^{3}MLCT state(s), and the other between the bright and mixed ^{3}MLCT states, as schematically shown in Figure 7a. If this is the case, then the emission intensity is expected to increase with temperature below the roll-over point, where the equilibrium between the weakly or nonemissive mixed and bright ^{3}MLCT states is believed to be dominant. Above the roll-over temperature, the equilibrium between the bright ^{3}MLCT state(s) and the ^{3}dd states predominates, such that a decrease in emission intensity with increasing temperature is observed. Within this model, the roll-over temperature should depend on the relative energy differences among the ^{3}dd states, the bright state(s), and the mixed state(s).

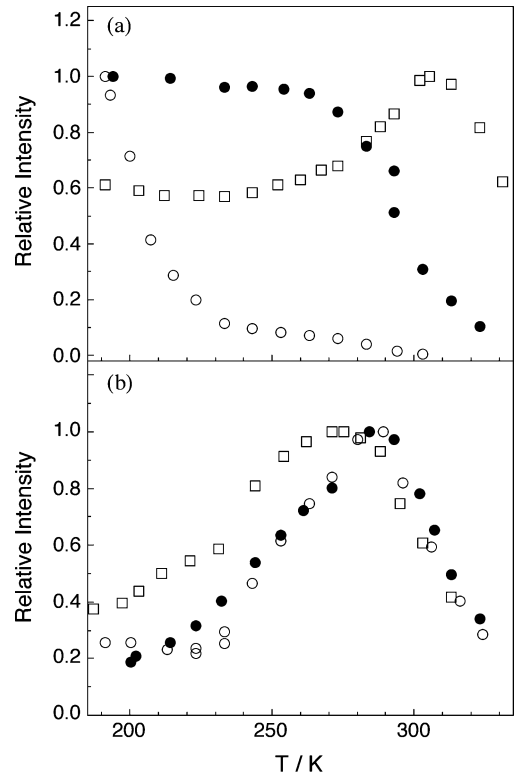

Figure 6. Changes in the relative integrated emission intensities of (a) **1** (●), **5** (○), and **6** (□), and (b) **2** (□), **3** (○), and **4** (●) as a function of temperature in ethanol.

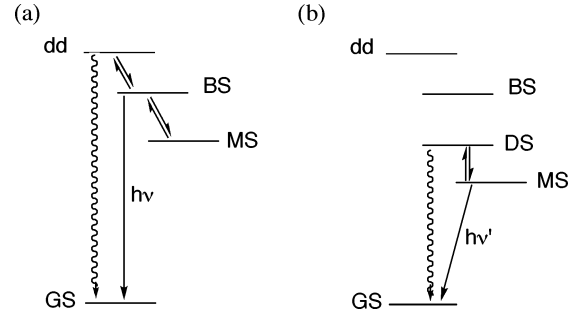

Figure 7. Schematic energy level diagram of excited states for (a) light-switch and (b) nonlight-switch complexes. GS: ground state; dd: ruthenium-based ^{3}dd state; BS: bright state; DS: dark state; MS mixed state.

(65) Onfelt, B.; Olofsson, J.; Lincoln, P.; Norden, B. *J. Phys. Chem. A* **2003**, *107*, 1000.

Since the ^{3}dd state is localized on the ruthenium center, it may be assumed that its energy is similar throughout the series **1**−**6**. In addition, the emission maxima of **1**−**4** and **6** lie in a relatively narrow region (615−635 nm in ethanol); therefore, it can also be assumed that the energy of the bright ^{3}MLCT states of these complexes is similar. Thus, it may be concluded that the differences observed in the temperature dependence of the emission among **2**−**4** and **6** stem from variations in the energy of the weakly or nonemissive mixed ^{3}MLCT state(s). These conclusions are supported by the calculated state energies shown in Figure 5.

In contrast to **2**−**4** and **6**, only a decrease in the emission intensity of **5** was observed with increasing temperature, such that a roll-over was not observed (Figure 6). It is evident from Figure 6 that the emission intensity of **5** decreases sharply from 190 to 230 K. As discussed above, the emission maximum of **5** is significantly red shifted at 298 K in CH_3CN, and its intensity is significantly weaker than those of **2**−**4** and **6** (Table 1, Figure S13, Supporting Information). A possible explanation for overall intensity, red shift, and the temperature dependence of **5** is that its weakly emissive lowest energy ^{3}MLCT state is in equilibrium with the nonemissive excited state (dark state) at higher energy, ES_2 ($\Delta E = 0.17$ eV), as schematically shown in Figure 7b. Unlike **2**−**4** and **6**, the emission from the lowest-energy state can be observed in **5** because its weak luminescence is not masked by that from low-lying excited states that are highly emissive.

Conclusions

Complexes **2**−**4** exhibit light-switch behavior similar to that of the prototype **6**, whereas **5** does not. This difference can be explained by the changes in the energy gap between the bright, highly emissive ^{3}MLCT excited state(s) that lie above and the lowest-energy ^{3}MLCT with mixed- or nonemissive character in these complexes. TD-DFT calculations show that, for the light-switch complexes, the lowest-energy MLCT state lies just below the bright state, such that the latter can be accessed thermally. In contrast, the lowest-energy MLCT state of **5** lies at significantly lower energy than the bright state, making the latter more difficult to populate at room temperature. The low-lying ^{3}MLCT state of **5** is weakly emissive and is in equilibrium with a dark state at higher energy, consistent with the calculations, electrochemistry, energy, and intensity of the luminescence in CH_3CN and the temperature dependence.

The optical measurements were conducted in CH_3CN to compare the experimental results to the calculation. It should be noted, however, that generally the emission maxima and intensities of light-switch complexes intercalated in DNA are similar to those in CH_3CN. The present work shows that **2**−**6** intercalate between the DNA bases; therefore, the difference in luminescence properties observed for **5** in the presence of DNA compared to **2**−**4** and **6** cannot be attributed to differences in DNA binding mode. Instead, the differences can be explained by the unique electronic structure of **5**.

Acknowledgement. C.T. thanks the National Science Foundation (CHE 0503666) and the Ohio Supercomputer Center. D.A.L. thanks the OSU for a University Presidential Graduate Fellowship.

Supporting Information Available: Syntheses and characterization, electronic absorption and excitation spectra, DNA binding constant fits, low-lying molecular orbitals, orbital contributions to low-lying electronic excited states. This material is available free of charge via the Internet at http://pubs.acs.org.

IC800560X